Contrasted release of insoluble elements (Fe, Al, rare earth elements, Th, Pa) after dust deposition in seawater: a tank experiment approach

Matthieu Roy-Barman, Lorna Foliot, Éric Douville, Nathalie Leblond, Frédéric Gazeau, Matthieu Bressac, Thibaut Wagener, Céline Ridame, Karine Desboeufs, Cécile Guieu

Biogeosciences, 18, 2663–2678, 2021
https://doi.org/10.5194/bg-18-2663-2021

Biogeosciences
Open Access
EGU

Contrasted release of insoluble elements (Fe, Al, rare earth elements, Th, Pa) after dust deposition in seawater: a tank experiment approach

Matthieu Roy-Barman[1], Lorna Foliot[1], Eric Douville[1], Nathalie Leblond[2], Fréderic Gazeau[3], Matthieu Bressac[3,4], Thibaut Wagener[5], Céline Ridame[6], Karine Desboeufs[7], and Cécile Guieu[3]

[1]Laboratoire des Sciences du Climat et de l'Environnement, LSCE/IPSL, CEA-CNRS-UVSQ, Université Paris-Saclay, Gif-sur-Yvette, France
[2]CNRS, Institut de la Mer de Villefranche, IMEV, Sorbonne Université, 06230 Villefranche-sur-Mer, France
[3]CNRS, Laboratoire d'Océanographie de Villefranche, LOV, Sorbonne Université, 06230 Villefranche-sur-Mer, France
[4]Institute for Marine and Antarctic Studies, University of Tasmania, Hobart, Tasmania, Australia
[5]CNRS, IRD, MIO, UM 110, Aix Marseille Univ., Université de Toulon, 13288 Marseille, France
[6]LOCEAN, Sorbonne Université, 4 Place Jussieu – 75252 Paris Cedex 05, France
[7]LISA, UMR7583, Université de Paris, Université Paris-Est-Créteil, Institut Pierre Simon Laplace (IPSL), Créteil, France

Correspondence: Matthieu Roy-Barman (matthieu.roy-barman@lsce.cnrs-gif.fr)

Received: 28 June 2020 – Discussion started: 21 July 2020
Revised: 4 February 2021 – Accepted: 24 February 2021 – Published: 27 April 2021

Abstract. Lithogenic elements such as aluminum (Al), iron (Fe), rare earth elements (REEs), thorium (^{232}Th and ^{230}Th, given as Th) and protactinium (Pa) are often assumed to be insoluble. In this study, their dissolution from Saharan dust reaching Mediterranean seawater was studied through tank experiments over 3 to 4 d under controlled conditions including controls without dust addition as well as dust seeding under present and future climate conditions (+3 °C and −0.3 pH). Unfiltered surface seawater from three oligotrophic regions (Tyrrhenian Sea, Ionian Sea and Algerian Basin) were used. The maximum dissolution was low for all seeding experiments: less than 0.3 % for Fe, 1 % for ^{232}Th and Al, about 2 %–5 % for REEs and less than 6 % for Pa. Different behaviors were observed: dissolved Al increased until the end of the experiments, Fe did not dissolve significantly, and Th and light REEs were scavenged back on particles after a fast initial release. The constant ^{230}Th/^{232}Th ratio during the scavenging phase suggests that there is little or no further dissolution after the initial Th release. Quite unexpectedly, comparison of present and future conditions indicates that changes in temperature and/or pH influence the release of Th and REEs in seawater, leading to lower Th release and a higher light REE release under increased greenhouse conditions.

1 Introduction

The ocean biological productivity is strongly controlled by the availability of trace metals such as iron (Fe), a limiting micronutrient for marine primary producers. Eolian dust deposition over the ocean represents a significant Fe source for marine ecosystems (Duce and Tindale, 1991; Jickells et al., 2005). However, eolian Fe fluxes are difficult to estimate because eolian dust fluxes, Fe solubility and dissolved Fe removal rates (by biotic and/or abiotic processes) are poorly constrained (Baker and Croot, 2010). To disentangle these processes, lithogenic tracers such as aluminum (Al), thorium (corresponding to ^{230}Th and ^{232}Th), protactinium (Pa) and rare earth elements (REEs) that are not affected by or are less affected by biological processes are used to determine lithogenic dust inputs (Measures and Vink, 2000; Hsieh et al., 2011; Greaves et al., 1999). This is based on the premise that surface water stocks of these lithogenic tracers should be more or less proportional to their release rate by the dis-

solution of eolian dust as long as they are not actively removed by the biological activity, scavenging and sedimentation. Moreover, thorium has one isotope (^{232}Th) derived from lithogenic material, whereas ^{230}Th is mostly produced in seawater by radioactive decay of conservative ^{234}U and hence can be used as a chronometer of the input and removal rate of ^{232}Th in ocean surface waters. A poorly constrained but key parameter for the application of these tracers is their dissolution rate from the lithogenic matrix into seawater (Anderson et al., 2016).

Here, we simulated Saharan dust deposition in surface Mediterranean seawater to determine the release of selected lithogenic tracers (Fe, Al, REEs, Th, Pa). The main objective was to determine the solubility of these tracers; their dissolution kinetics; and the possible influence of temperature, pH and biological activity on the dissolution processes. Dust deposition was simulated in tanks filled with unfiltered seawater (to retain the impact of biological activity) with an added amount of dust corresponding to a strong Saharan dust deposition event over the Mediterranean Sea.

2 Methods

2.1 Experimental setup

A detailed description of the artificial dust addition experiments is given in Gazeau et al. (2020). Briefly, six experimental high-density polyethylene (HDPE) tanks (300 L each) with a conical base connected to a sediment trap were installed in a temperature-controlled container during the PEACETIME cruise (https://doi.org/10.17600/17000300). The cruise was conducted on board the R/V *Pourquoi Pas?* in the Mediterranean Sea during the late spring, a period characterized by strong stratification (Guieu et al., 2020a). Three stations representing different in situ conditions, albeit all characterized by oligotrophic conditions, were chosen to conduct the tank experiments: stations TYR in the Tyrrhenian Sea, ION in the Ionian Sea and FAST in the Algerian Basin (Fig. S1; Guieu et al., 2020a). Experiments at TYR and ION lasted 3 d (72 h), while the last experiment (at station FAST) was extended to 4 d (96 h). The experimental tanks were filled with unfiltered seawater from the continuous surface pumping system upon arrival at stations TYR (17 May 2017) and ION (25 May 2017) and 1 d after arrival at station FAST (2 June 2017). This was done using a large peristaltic pump (Verder VF40 with an ethylene propylene diene monomer (EDPM) rubber hose, flow of 1200 L h^{-1}) collecting water 5 m below the base of the boat. Tanks C1 and C2 were unmodified control tanks, and tanks D1 and D2 were enriched with dust at the beginning of the experiment (3.6 g of dust per tank; 10 g m^{-2} was sprayed over each tank during 20 min, typical of the intermittent but strong Saharan dust deposition event over the Mediterranean Sea; see Sect. 4). Tanks G1 and G2 were enriched with dust as in tanks D1 and D2 but incubated at a higher temperature (+3 °C) and with lower pH (−0.3 pH). The atmosphere above tanks C1, C2, D1 and D2 was flushed with ambient air. Tanks G1 and G2 were flushed with air enriched with 1000 ppm CO_2 in order to prevent CO_2 degassing. The height of the tank (1.1 m) allowed the settling of the particles to be taken into account and the analysis of a series of parameters in suspended and sinking matter.

Dust particles were derived from the fine fraction (< 20 µm) of a Saharan soil (Tunisia) processed physically and chemically (including a treatment simulating the effect of cloud water and evapo-condensation) to produce an analogue of Saharan dust deposited over the Mediterranean Sea (see details in Guieu et al., 2010). The size spectrum of the treated dust has a median diameter around 6.5 µm and a peak at approximately 10 µm similar to the one found in Mediterranean aerosols (Guieu et al., 2010). It is a mixture of quartz (40 %), calcite (30 %) and different clay minerals (25 %) with 3.3 % Al and 2.3 % Fe by weight (Desboeufs et al., 2014). The detailed dust seeding procedure is described in Gazeau et al. (2020a). At station TYR, samples for dissolved Fe and Al were taken at $t = 0$ (before enrichment) and at $t = 1$, 24 and 72 h after dust enrichment. No samples for rare earth elements (REEs), Th and Pa were taken at this station. At station ION, all tanks were sampled for Al, Fe, Th and REEs at $t = 1$, 24 and 72 h after dust addition. At station FAST, tanks C1 and D1 were sampled for Al, Fe, Th, Pa and REEs at $t = 0$, 1, 6, 12, 24, 48, 72 and 96 h after dust addition. At this station, tanks C2, D2, G1 and G2 were sampled for Al, Fe, Th and REEs at $t = 1$, 48 and 96 h after dust enrichment.

At the end of each experiment, the particulate material that settled at the bottom of the tanks was recovered from the sediment traps and preserved by adding formaldehyde (5 % v/v final concentration).

2.2 Analytical techniques

2.2.1 Dissolved Fe

Dissolved iron (DFe) concentrations were measured by flow injection with online preconcentration and chemiluminescence detection (Bonnet and Guieu, 2006; Guieu et al., 2018). An internal acidified seawater standard was measured daily to control the stability of the analysis. The detection limit was 15 pM, and the accuracy of the method was controlled by analyzing the following seawater samples: SAFe S (consensus value 0.093 ± 0.008 nmol kg^{-1}), SAFe D1 (consensus value 0.67 ± 0.04 nmol kg^{-1}), GD (consensus value 1.00 ± 0.10 nmol kg^{-1}) and GSC (consensus value not available) seawater standards. Average values measured during this study were 0.086 ± 0.010 nmol kg^{-1} ($n = 3$) for SAFe S, 0.64 ± 0.13 nmol kg^{-1} ($n = 19$) for SAFe D1, 1.04 ± 0.10 nmol kg^{-1} ($n = 10$) for GD and 1.37 ± 0.16 nmol kg^{-1} ($n = 4$) for GSC.

2.2.2 Dissolved Al

Determinations of dissolved aluminum (DAl) concentrations were conducted on board using the fluorometric method described by Hydes and Liss (1976). After filtration, samples were acidified to pH < 2 with double-distilled concentrated HCl. After at least 24 h, lumogallion reagent was added to the sample, which was then buffered to pH = 5 with ammonium acetate. The sample was then heated to 80 °C for 1.5 h to accelerate the complex formation. The fluorescence of the sample was measured with a Jasco FP 2020 + spectrofluorometer (excitation wavelength 495 nm, emission wavelength 565 nm). The detection limit varied between 0.2 and 0.5 nM and the blank values between 0.9 and 1.7 nM for the different days of analysis. Based on the daily analysis of an internal reference seawater standard, the overall variability in the method was 0.6 nM (the standard deviation of a mean concentration of 53.5 nM, $n = 25$).

2.2.3 Dissolved REEs, Th and Pa

Seawater was sampled from the tanks and filtered (pore size 0.2 µm; Sartobran®) within 1 to 2 h after sampling and subsequently acidified with trace-metal-grade HCl (NORMATOM®). Approximately 250 mL of filtered and acidified seawater was spiked with isotopes ^{150}Nd, ^{172}Yb, ^{229}Th and ^{233}Pa for isotope dilution measurements followed by $KMnO_4$ and $MnCl_2$ addition. REEs, Th and Pa were preconcentrated by MnO_2 co-precipitation obtained after raising pH to 8 through addition of concentrated NH_3. The MnO_2 precipitate was recovered by filtration onto a 25 mm cellulose ester filter, rinsed with Milli-Q water and dissolved in a solution composed of 2 mL of 6 N HCl and 10 µL of H_2O_2. Thereafter, REEs, Th and Pa were separated using an AG1X8 ion exchange column (Gdaniec et al., 2018).

REE contents were measured at the Laboratoire des Sciences du Climat et de l'Environnement (LSCE) by using a quadrupole induced coupled plasma mass spectrometer (ICPMS) (Xseries^{II}, Thermo Scientific©). Nd and Yb concentrations were directly determined by isotope dilution. Comparison of Nd and Yb concentrations measured by isotope dilution with the concentration determined by internal calibration (using In-Re internal standard) provided a yield of the chemical procedure for Nd and Yb (between 70 % and 100 %). The chemical yields for Nd and Yb were used to estimate those of the other REEs, by assuming that the yield is a linear function of the atomic number (Arraes-Mescoff et al., 2001).

Pa and Th analyses were performed using an inductively coupled plasma mass spectrometer (MCICP-MS; Neptune^{plus}©) equipped with a secondary electron multiplier (SEM) and a retarding potential quadrupole (RPQ) energy filter (Gdaniec et al., 2018).

Analyses of seawater used during the GEOTRACES intercalibration exercise (van de Flierdt et al., 2012) showed agreements within a few percent with consensual REE values, except for La and Lu, which were underestimated by 25 % and 10 % (Table S1 in the Supplement). Agreement within analytical uncertainties was obtained for ^{232}Th and age-corrected ^{230}Th concentrations. The very large uncertainties in ^{232}Th analyses of the GEOTRACES standard were due to its low ^{232}Th content (in particular when compared to Mediterranean seawater and the small sample volume used). Values of ^{231}Pa are not reported for these intercalibration samples because of the encountered yield and blank problems (see Sect. 3.5).

2.2.4 Trapped particles

Samples were collected following the standard protocol developed at the national service "Cellule Piege" of the French INSU-CNRS (Institut National des Sciences de l'Univers of the Centre National de la Recherche Scientifique) (Guieu et al., 2005). Trapped particles were rinsed three times with ultrapure (Milli-Q) water in order to remove salt and freeze-dried. Approximately 10 mg of trap-collected sediment was then weighed and acid-digested with HNO_3–HF using Suprapur reagents at 150 °C in PTFE vials. After complete acid evaporation, samples were diluted in 0.1 M HNO_3 and analyzed for Fe and Al concentrations by induced coupled plasma atomic emission spectroscopy (ICP-AES) (JY 138 "Ultrace", Jobin Yvon). A fraction of the remaining solution was used to analyze REEs, Th and Pa. Before Th and Pa analysis, the solution was spiked with ^{229}Th and ^{233}Pa and treated through the same chemical process as the Mn precipitate used for the dissolved Pa and Th analysis. REEs were analyzed directly on a quadrupole ICPMS (Xseries^{II}, Thermo Scientific) using an internal calibration (Re).

3 Results

3.1 Dissolved Fe

Over the course of the three experiments, DFe concentrations in control tanks were in the range of 0.7–2.5 nM (Table S2 in the Supplement, Fig. 1), in good agreement with DFe measured during the cruise in surface waters between 0 and 15 m depth (TYR: 1.47 ± 0.30; ION: 1.41 ± 0.19; FAST: 1.71 ± 0.35 nM; Bressac et al., 2021) and with surface concentrations observed in the Mediterranean Sea during the stratification period (Bonnet and Guieu 2006; Gerringa et al., 2017; Wagener et al., 2008). For the TYR experiment, there was no clear difference between controls (C1 and C2) and dust-amended tanks (D1, D2, G1 and G2) that would indicate significant Fe release from dust. During the ION experiment, DFe concentrations measured in G1 were much higher than in the other tanks, most likely due to a contamination issue. DFe concentrations were lower in control tanks than in dust-amended tanks during the FAST experiment. However, here

too, high variability between duplicates suggests possible Fe contamination during sampling or sample processing.

3.2 Dissolved Al

Al concentrations in control tanks varied between stations (47 ± 3 nM at TYR, 77 ± 5 nM at ION and 25 ± 2 nM at FAST; Table S2, Fig. 1), with little variability between tanks at individual stations. These values are within the range of concentrations observed in Mediterranean surface waters (Rolison et al., 2015). After dust addition, Al concentrations increased linearly with time in treatments D and G at all stations, reaching final concentrations 50 to 100 nM higher than in control tanks. No systematic differences between D and G treatments were observed. The increase in Al at FAST (72–80 nM) was larger than at TYR and ION (52–68 nM) due to the longer duration of the FAST experiment.

3.3 Dissolved rare earth elements

The REE concentrations measured in control tanks at stations ION and FAST (Table S3 in the Supplement, Fig. 2) compared well with values reported in the Mediterranean Sea (Censi et al., 2004; Tachikawa et al., 2004). In control tanks at both ION and FAST, a slight increase in REE concentrations during the course of the experiments indicated some contamination from the tank or the environment of the experiment. The potential contamination remained low (i.e., from 15 % to 40 % of the initial value for dissolved Nd, from 5 % to 10 % of the initial value for dissolved Yb) compared to changes in concentrations observed in the dust-amended tanks. For both D and G, there was a sharp increase in the concentrations of all REEs (i.e., around +400 % for dissolved Nd and +100 % for dissolved Yb), followed by a slow decline in light REEs (LREEs; such as Nd; Fig. 2), while heavy REE concentrations (HREEs; e.g., Yb; Fig. 2) remained constant. The rapid increase in REE concentrations can be observed by comparing the REE concentrations at $t = 0$ (before dust seeding) and $t = 1$ h during the D1 experiment at FAST. For the other experiments (including the ION tanks), the comparison of the D or G concentrations at $t = 1$ h after dust seeding with the concentrations recorded in the C series (no seeding) also highlights a sharp increase in the REE concentrations. The only exception in these trends was observed at FAST for tank D2, where no increase in REE concentrations was observed after dust addition ($t = +1$ h). As this most likely resulted from a technical issue during sampling (perhaps bottle labeling), we consider this value to be an outlier. In general, at any given time and site, REE concentrations were somewhat higher in the warmer and acidified tanks (G) as compared to ambient environmental conditions (D). The subsequent decrease in concentrations was steeper for LREEs (e.g., Nd, for which the concentration decrease was visible as early as $t = +6$ h) than for HREEs (e.g., Yb, for which the concentration remained relatively constant after $t = +1$ h).

3.4 Dissolved thorium isotopes

Concentrations of ^{232}Th in control tanks remained around 1 pM during the incubations at both FAST and ION (Table S3, Fig. 3), in agreement with surface water concentrations in the Mediterranean Sea (Gdaniec et al., 2018). A higher ^{232}Th concentration (10.9 ± 0.1 pM) was measured in tank C1 at the FAST station 12 h after the start of the experiments (10.9 pM). Since the consecutive measurement for this tank was in the expected range (1.5 pM), this extreme value likely resulted from a sample contamination rather than a contamination of the tank itself. As observed for the REEs, there was a sharp increase in ^{232}Th concentrations after dust addition at both ION and FAST. Concentrations after 12 and 24 h of incubation at station FAST were higher in tank D1. However, as described above for tank C1 at station FAST and for the sampling time $t = +12$ h, we consider that these high values can be attributed to sample contamination during sampling. Therefore, we do not consider these two samples further in the discussion (Fig. 3).

After the rapid ^{232}Th increase in the D and G treatments at FAST and ION, a rapid and significant decrease in the ^{232}Th concentrations was observed. In contrast to REEs, ^{232}Th concentrations were higher in the D tanks than in the G tanks.

The variations in ^{230}Th concentrations with time and between treatments were more or less similar to ^{232}Th. However, significant variations in the ^{230}Th/^{232}Th ratio were observed (Table S3, Fig. 3, Fig. S3 in the Supplement). The highest ratios ($\geq 10 \times 10^{-6}$ mol mol^{-1}) were measured in the control tanks.

3.5 Dissolved protactinium

Due to analytical problems (low yield and large blanks), largely because of the small sample volumes available and the low Pa content in the Mediterranean surface water, reliable Pa concentrations could only be obtained at FAST in tanks C1 and D1. The mean ^{231}Pa concentrations at FAST were not different within uncertainties in the C1 (2.5 ± 0.2 aM, with 1 aM $= 10^{-18}$ M) and D1 (2.4 ± 0.2 aM) treatments (Table S3 in the Supplement, Fig. 4). Despite the small volumes of seawater analyzed, these concentrations agree within uncertainties with the Pa concentrations available for western Mediterranean Sea surface waters (Gdaniec et al., 2018). Due to the relatively large uncertainties in the individual data, no systematic temporal trend could be detected.

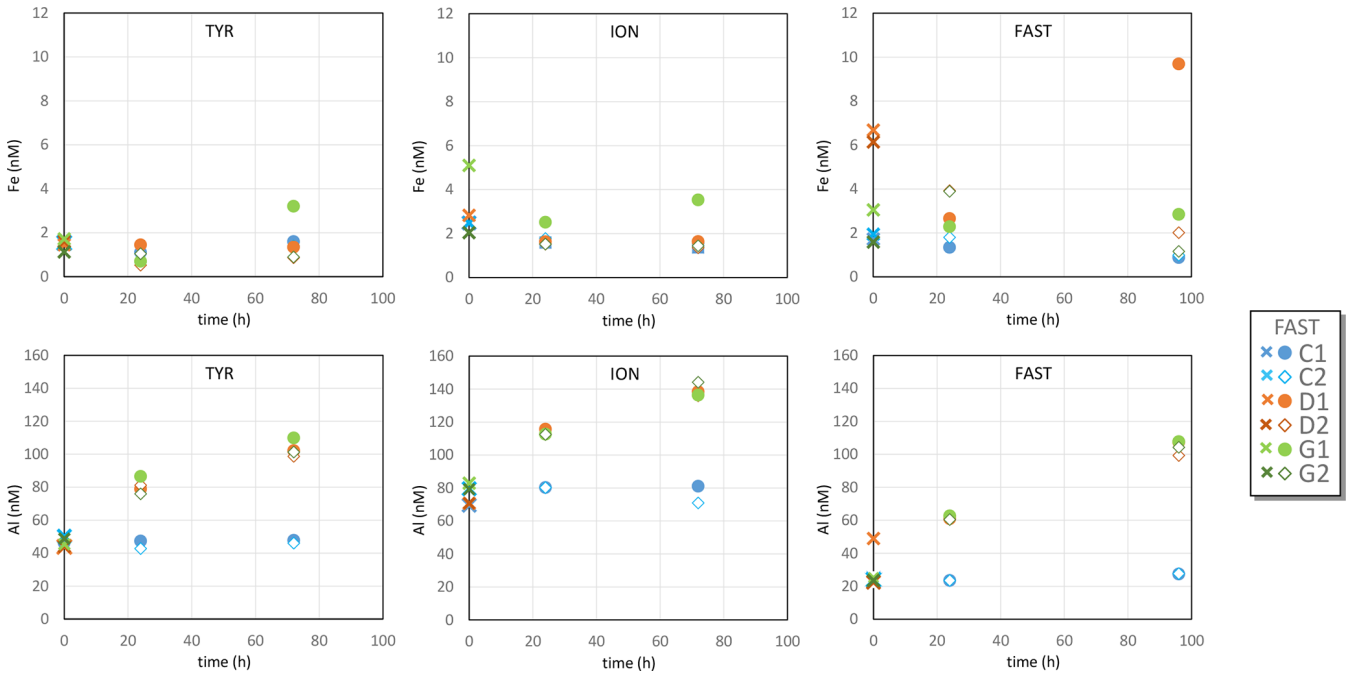

Figure 1. Concentrations of total dissolved Fe and Al during the dust addition experiments. Crosses correspond to samples collected before dust addition ($t = 0$).

3.6 Trapped material

The material collected in the traps contained 2.59 % ± 0.03 % (weight percent; 1 standard deviation, $n = 12$) Fe and 4.8 ± 0.1 % (1 standard deviation, $n = 12$) Al (Table S4 in the Supplement). These concentrations are significantly higher than the initial dust composition (2.26 ± 0.03 % of Fe and 3.32 ± 0.03 % of Al) due to preferential dissolution of highly soluble calcium carbonate or possibly calcium hydrogen carbonate formed during the simulation of dust processing in clouds (see Sect. 2.1; Desboeufs et al., 2014). The Ca (14.0 % ± 0.02 %) content was lower in the trapped material compared to the initial dust (16.54 % ± 0.16 %) due to calcium carbonate dissolution, indicating a dissolution of 18 % of the carbonates initially present or 6.4 % of the dust mass. REE concentrations in the sediment trap (Table S5 and Fig. S2 in the Supplement) were close to concentrations for the average upper continental crust (Taylor and McLennan, 1995). Particulate ^{232}Th concentrations corresponded to 70 ± 5 % of the upper continental crust concentration. The ^{230}Th concentrations corresponded roughly to secular equilibrium for a U/Th ratio of 0.363 ± 0.008 g g^{-1}, within the range observed in average continental crust. The ^{231}Pa concentrations corresponded to secular equilibrium for a U/Th ratio of 0.330 ± 0.045 g g^{-1}, also within the range of the continental crust and Saharan aerosols (Pham et al., 2005).

4 Discussion

The concentration changes observed during the experiments resulted from a net balance between the release of chemical elements by the dissolution of the added dust and removal of these elements by particle scavenging and sedimentation or active (biological) uptake. For Fe, the scavenging efficiency largely depends on Fe solubility driven by Fe-binding ligands (Witter et al., 2000). As the dust concentration in tanks was high, Fe re-adsorption on dust particles could have been an important scavenging process (Wagener et al., 2010). Dust inputs over the Mediterranean Sea are very irregular (Loÿe-Pilot and Martin, 1996). The dust quantity used for the seeding (10 g of total dust m^{-2} with an Al content of 4 %) corresponds to half of the highest dust pulse observed during one rain event in the Mediterranean (e.g., Ternon et al., 2010) and represents 30 %–100 % of the annual dust deposition over the Mediterranean Sea (Guieu et al., 2010). Hence, the PEACETIME experiments also document the yearly release of insoluble elements in the Mediterranean surface waters.

4.1 Solubility of tracers

The soluble fraction (%) of the different elements was calculated as the maximum release of the considered element during the experiments divided by the amount of particulate element per volume of seawater introduced in the tanks by

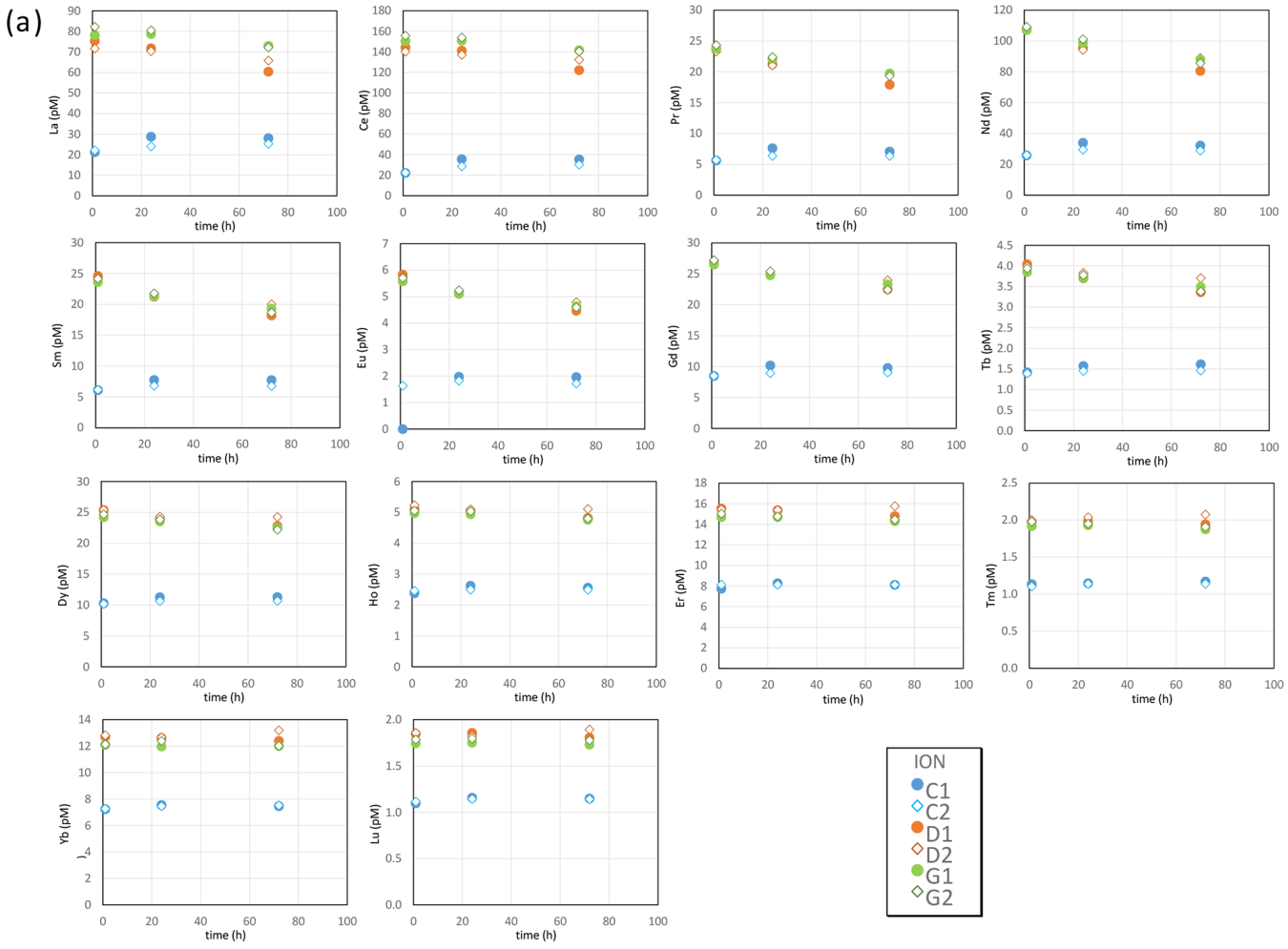

Figure 2.

dust addition (Table 1) following the equation:

$$f_{\text{dissol\_conc}} = \frac{\text{CONC}_{\text{max}} - \text{CONC}_{\text{init}}}{\text{CONC}_{\text{dust}} \times m/V} \times 100, \quad (1)$$

where $f_{\text{dissol\_conc}}$ is the soluble fraction of the element, $\text{CONC}_{\text{init}}$ is the dissolved concentration before dust input (estimated with the concentration in the C tanks measured at $t = 1$ h and averaged over tank replicates 1 and 2), CONC_{max} is the maximum concentration measured during the experiment (concentration in the D or G tanks measured at $t = 1$ h and averaged over tank replicates 1 and 2), $\text{CONC}_{\text{dust}}$ is the concentration in the original dust (expressed in mol of insoluble element g^{-1} of dust), m represents the mass of dust added to the tank (3.6 g), and V represents the volume of seawater in the tank (300 L). Direct analysis of the original dust was used for total Fe and Al (Guieu et al., 2010). REEs, Th and Pa were not analyzed in the initial dust material. For these elements, we used the average concentrations of particles collected in the traps assuming that

- REE, Th and Pa concentrations in the added dust were identical to the sedimented material;
- for REEs, Th and Pa, the contribution of plankton and other biogenic material produced during the experiment to the sedimented material was negligible due to the high dust load recovered in the trap;
- carbonate dissolution (see Sect. 3.6) had a negligible effect on the particulate concentration of REEs, Th and Pa.

We estimated $f_{\text{dissol\_conc}}$ considering the total mass of dust added to the tank rather than the dust remaining in suspension at the end of the experiment in order to relate the amount of element released in seawater to the total flux of dust deposited at the sea surface. At the end of the experiments, the dust loss by sedimentation in the traps ranged from 33 % to 80 % of the total mass of dust added to each tank (m), likely depending on the intensity of aggregation in each tank (as previously observed by Bressac et al., 2012). However, these

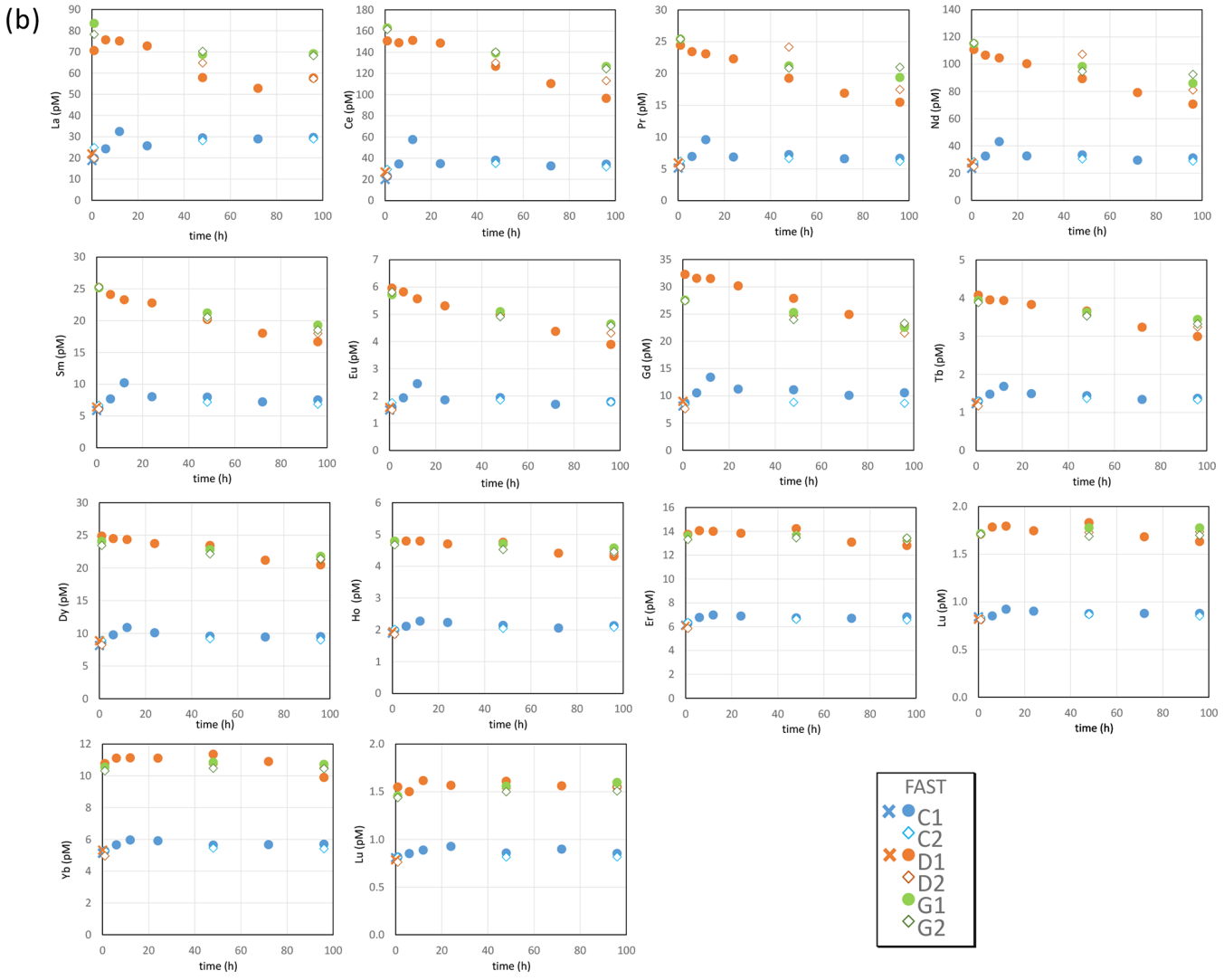

Figure 2. Concentrations of dissolved REEs during the tank experiments at **(a)** ION station and **(b)** FAST station. Crosses correspond to samples collected before dust addition ($t = 0$).

differences did not seem to impact the estimation of the soluble fraction significantly. For example, at the ION station, while a large difference was observed between the amount of Al collected in the sediment traps of D1 and D2 (when seeding, 74 % and 33 % of the Al introduced were recovered in the traps, respectively, so that only 25 % and 67 % of the initial particulate remained in suspension at the end of the experiment), the soluble fractions were identical in D1 and D2 for all the studied elements (Figs. 1–3, Table 1). This reflects the fast dissolution for these elements.

During the experiments, the DFe concentrations were probably affected by contaminations. Nevertheless, we can assess the upper limit to Fe dissolution by assuming that the highest DFe concentrations measured during the experiments truly represented Fe dust release. The highest DFe (10 nM) was measured at the FAST station in the dust-amended tank D1 at $t = 72$ h. Given that 30 µM of particulate Fe ($CONC_{dust}$ for Fe) was added to each tank, Fe dissolution would be at most 0.3 %. This result is in good agreement with the soluble fraction of Fe obtained using the same dust and tanks filled with filtered abiotic coastal northwestern Mediterranean seawater in May (Bressac and Guieu, 2013; Louis et al., 2018).

No significant differences in ^{231}Pa concentrations between C1 and D1 at FAST were observed. Based on trap analyses (Table S5), we estimate that 0.04 fM of ^{231}Pa was added to the tanks. Given the analytical uncertainties in dissolved ^{231}Pa analysis (Fig. 4), $CONC_{max} - CONC_{init}$ is certainly below 0.002 fM. Hence, the soluble fraction of ^{231}Pa is below 5 %. As expected for these poorly soluble elements, the maximum soluble fractions were low for all stations: less than 0.3 % for Fe, 1 % for ^{232}Th and Al (although their dissolution

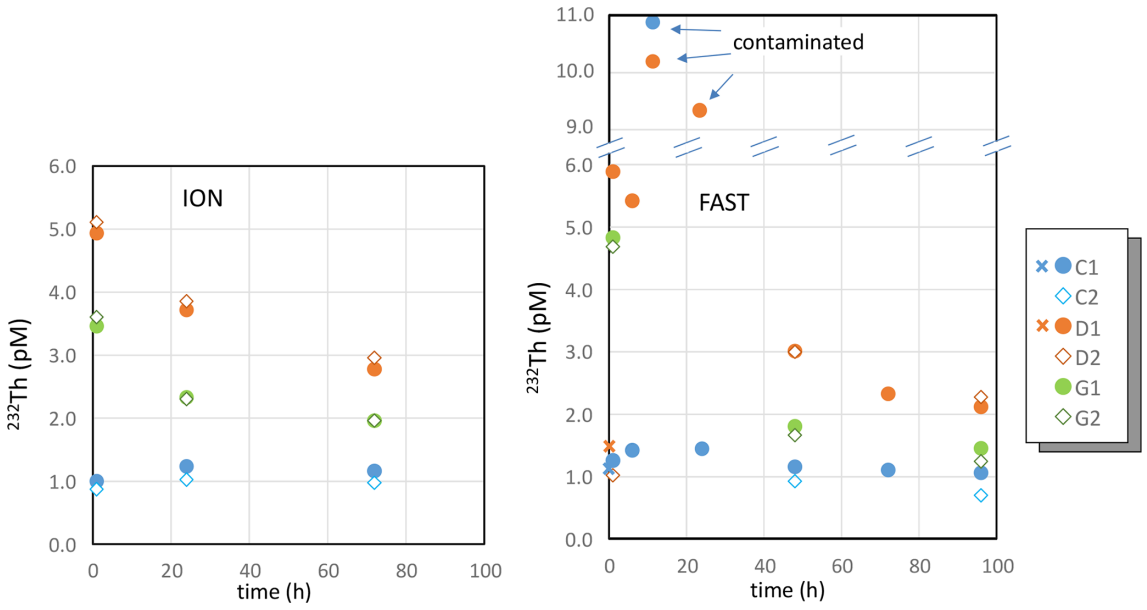

Figure 3. Dissolved ^{232}Th during the ION and FAST experiments. Note the break in the y axis so as to include values of the three outliers (contaminated samples). Crosses correspond to samples collected before dust addition ($t = 0$).

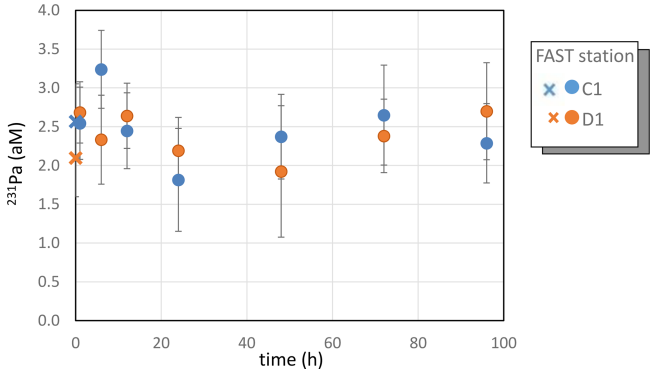

Figure 4. Dissolved Pa during the FAST experiments. Error bars correspond to the analytical uncertainties ($2\sigma_n$, where σ_n is the error of the mean). Crosses correspond to samples collected before dust addition ($t = 0$).

kinetics do not have the same patterns), and about 2 %–5 % for REEs.

Al dissolution was slightly higher at FAST compared to ION and TYR but identical in the D and G treatments. The contrasting behaviors of Al that progressively dissolved during the experiments and Fe that did not dissolve significantly may be due to their respective solubility. The Al concentrations (22–144 nM) during the experiments were much lower than the dissolved Al concentration in seawater at equilibrium with Al hydroxides, which is at the micromolar level (Savenko and Savenko, 2011). By contrast, dissolved Fe concentrations during the experiments were close to or above the theoretical solubility of Fe hydroxides in seawater (Millero, 1998; Wagener et al., 2008). For Al (as well as for Fe), there was no sample analyzed for $t = 1$ h (just after dust addition), so it was not possible to detect a putative early dissolution as observed for REEs and Th (see below).

In contrast to Al, both Th and REEs were released rapidly after dust addition, similarly to phosphate and nitrate (Gazeau et al., 2020). Fortuitously or not, it appears that more Th and dissolved inorganic phosphorus (DIP) were released at FAST than at ION. Among the differences between ION and FAST, we note a higher biomass (chlorophyll a at the end of the experiments: $0.48 \pm 0.08\,\mu g\,kg^{-1}$ for FAST and $0.26 \pm 0.08\,\mu g\,kg^{-1}$ for ION) and a lower alkalinity ($2452 \pm 5\,\mu mol\,kg^{-1}$ for FAST and $2626 \pm 4\,\mu mol\,kg^{-1}$ for ION; Gazeau et al., 2020) for FAST compared to ION; ^{232}Th was mostly released in the very beginning of the incubations. At both FAST and ION, Th dissolution was higher in the D tanks than in the G tanks (Fig. 2). In contrast, highest biomass was found in the G tanks (Gazeau et al., 2020). The higher incubation temperature for the G tanks resulted in higher concentrations of transparent exopolymeric particles (TEPs; Gazeau et al., 2021). The high affinity of Th for TEPs (Santschi et al., 2006) could have led to the lower Th concentrations in these tanks. At present, however, it is not possible to determine with certainty what caused the low percentage of Th release in the G tanks as compared to the D tanks.

The soluble fractions of REEs were similar at FAST and ION. However, slightly lower LREE dissolution fractions occurred under ambient environmental conditions (D; 1.6 % for La) than under future conditions (G; 1.9 % for La). The soluble fraction of REEs increased almost linearly between elements from La (1.7 ± 0.2 %) to Dy (4.6 ± 0.2 %) and then de-

Table 1. Maximum fractional dissolution and scavenging in percent.

	Fe	Error	Al	Error	La	Error	Ce	Error	Pr	Error	Nd	Error	Sm	Error	Eu	Error	Gd	Error	Tb	Error	Dy	Error	Ho	Error	Er	Error	Tm	Error	Yb	Error	Lu	Error	Th_{conc}	Th_{sol} * (range)	Pa
Dissolution fraction in percent																																			
TYR_D	0.01	0.01	0.56	0.05																															
TYR_G	0.02	0.02	0.82	0.27																															
ION_D	0.01	0.01	0.91	0.04	1.6	0.2	1.9	0.2	2.4	0.2	3.0	0.2	3.4	0.3	3.8	0.2	3.7	0.2	4.2	0.2	4.5	0.3	4.7	0.5	4.3	0.3	3.7	0.4	3.5	0.3	3.5	0.3	1.02	0.17	0.7	(0.64–0.73)	
ION_G	0.03	0.03	0.96	0.09	1.9	0.2	2.1	0.1	2.5	0.2	3.1	0.2	3.4	0.2	3.7	0.1	3.8	0.2	4.1	0.2	4.3	0.2	4.6	0.3	4.2	0.4	3.7	0.4	3.2	0.1	3.2	0.3	0.66	0.05	1.1	(1.0–1.2)	
FAST_D	0.10	0.04	1.09	0.08	1.6	0.1	1.9	0.2	2.5	0.3	3.1	0.3	3.5	0.4	4.0	0.5	4.8	0.6	4.5	0.5	4.7	0.5	4.8	0.5	4.5	0.5	3.8	0.6	3.5	0.4	3.5	0.4	1.19	0.03	0.1	(0–8)	< 6 %
FAST_G	0.04	0.01	1.13	0.03	1.8	0.3	2.1	0.3	2.6	0.3	3.3	0.3	3.5	0.2	3.7	0.2	3.9	0.2	4.3	0.2	4.7	0.2	5.0	0.3	4.5	0.3	3.8	0.1	3.5	0.2	3.1	0.1	0.91	0.11	2.4	(1–7)	
Scavenging fraction in percent																																			
ION_D 72 h					14.2	8.3	10.6	6.9	20.5	6.0	21.4	6.2	21.7	6.2	19.9	5.1	13.9	4.7	12.0	6.8	7.3	4.3	4.0	5.7	1.4	4.8	−1.2	5.6	−0.3	5.2	0.1	3.8	43	4		
ION_G 72 h					9.5	3.9	7.9	2.7	18.8	2.7	19.7	2.7	20.4	3.3	18.2	1.9	14.8	4.0	11.9	3.4	8.7	2.0	4.6	1.7	3.2	2.3	2.9	3.3	0.9	0.3	0.7	3.5	45	2		
FAST_D 72 h					25.2	6.1	26.7	6.2	30.9	5.9	28.5	5.8	28.6	6.7	26.6	8.1	22.8	7.4	20.6	7.3	14.9	8.0	7.8	9.1	4.7	9.0	1.6	9.7	4.2	8.6	3.0	10.2	64	2		
FAST_D 96 h					18.3	5.9	35.9	4.8	36.7	5.0	36.2	4.7	33.9	7.1	34.7	8.0	29.3	7.1	26.5	7.3	17.7	8.4	9.8	9.6	6.8	9.8	4.6	10.5	12.8	8.5	3.6	10.8	60	1		
FAST_G 96 h					15.1	4.6	22.7	1.4	20.6	4.5	22.6	4.3	25.1	2.3	20.0	1.7	16.6	2.2	13.5	2.9	9.1	2.9	4.5	3.4	0.5	2.1	−1.4	3.5	−1.5	3.5	−7.3	5.3	72	4		

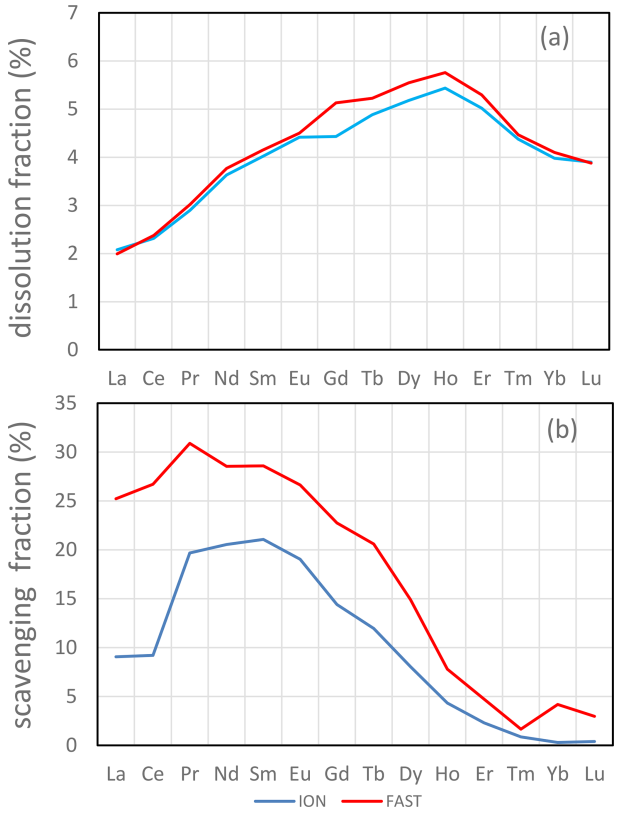

Figure 5. (a) Average maximum dissolution ($f_{\text{dissol\_conc}}$, given in percent) and **(b)** scavenging fractions (f_{scav}, given in percent) for REEs. For comparison purposes, scavenging was calculated with data at $t = 72$ h for both ION and FAST.

creased for heavier elements (3.3 ± 0.2 % for Lu; Fig. 5a). It closely follows the solubility pattern obtained from Saharan aerosols leached with filtered seawater (Greaves et al., 1994). In this study, the pattern of the soluble fraction of REEs was associated with Fe oxyhydroxides and exceeded the soluble fraction of Fe, possibly due to the high REE content of Fe oxyhydroxides (Haley et al., 2004).

An unexpected result of the PEACETIME experiments is the contrasting dissolution kinetics of Al relative to Th and REEs. Specific REE- and Th-rich phases may partly account for the decoupling with Al (Marchandise et al., 2014). Alternatively, the fast dissolution of calcium carbonate or calcium hydrogen carbonate formed during dust processing to simulate clouds might account for the REE and Th release (see Sects. 3.6 and 4.3).

The soluble fraction of Mediterranean aerosols was also evaluated by leaching aerosols collected during the PEACETIME cruise in ultrapure water for 30 min (van Wambeke et al., 2020). The median soluble fraction of Nd was 6 %, close to the soluble fraction of Nd in our tank experiments (3 %). These low values are also consistent with former estimates based on Saharan aerosol leaching in distilled water (1 %–3 %; Greaves et al., 1994). In contrast, aerosol leaching

in ultrapure water during PEACETIME by Fu et al. (2021) suggested much larger Al and Fe solubilities (around 20 %) than those observed during our dust addition experiments. These differences reflect mainly the anthropogenic component in the aerosol samples collected during the cruise, resulting from mixing of Saharan dusts and polluted air masses (Fu et al., 2021). Anthropogenic metals are significantly more soluble than metals issued from desert dust (Desboeufs et al., 2005). However, the Al and Fe solubility values obtained in our dust addition experiments are in agreement with the values found in ultrapure water for the same amended dust (Aghnatios et al., 2014), for other Saharan dust analogs (Desboeufs et al., 2001; Paris et al., 2011) or for dust collected over the Sahara (Paris et al., 2010). We conclude that the solubility of particulate Al and Fe obtained in our experiments is representative of pure Saharan dust inputs.

4.2 Removal of dissolved tracers

During the experiments, biological uptake or scavenging onto particulate matter may have biased the soluble-fraction estimates for the less soluble elements. Fe and Al are well known for being taken up by plankton as a micronutrient (e.g., Twining et al., 2015) and Al by substitution to Si in diatom frustules (Gehlen et al., 2002). With the chlorophyll *a* (chl *a*) increase observed during the course of the experiments (at most $0.5\,\mu g\,L^{-1}$), a C/chl *a* ratio of $50\,mg\,C\,(mg\,chl\,a)^{-1}$ and an Fe/C ratio ranging from 10 to $100\,\mu mol\,mol^{-1}$ (Twining et al., 2015), we estimate that biological activity should have taken up at most 0.25 nM of Fe, an order of magnitude less than the dissolved Fe measured during the course of the experiments. Therefore, any significant Fe dissolution would not have been masked by biological uptake. Using the biogenic silica flux measured in the sediment traps ($10–41\,mg\,m^{-2}\,d^{-1}$) and an Al/Si ratio in diatom frustules of 0.008 (maximum value in Gehlen et al., 2002), diatoms could have incorporated as much as 6–18 nM Al. This represents a small but significant fraction of the Al released by the dust.

As REEs and Th are not known to be taken up by plankton, their decreasing concentrations during the course of the experiments suggest that they may be removed by scavenging onto particles. We define the scavenging fraction as follows:

$$f_{scav} = \frac{CONC_{max} - CONC_{min}}{CONC_{max}} \times 100, \quad (2)$$

where f_{scav} is the scavenging fraction of the element, $CONC_{max}$ is the dissolved concentration measured at the beginning of the incubation ($t = 1$ h) averaged over tanks 1 and 2 of the D or G experiments, and $CONC_{min}$ is the dissolved concentration measured at the end of the incubation ($t = 72$ h or $t = 96$ h) averaged over tanks 1 and 2, except for FAST D ($t = 72$ h; measured in tank 1 only). Th appeared to be the element most sensitive to scavenging ($f_{scav} = 43\,\%–44\,\%$ at ION and 65 %–70 % at FAST). REE scavenging was less prominent and decreased from LREEs ($f_{scav} = 15\,\%–37\,\%$) to HREEs ($f_{scav} = 1\,\%–13\,\%$; Fig. 5b). The reduced scavenging of HREEs is consistent with the stronger complexation of HREEs by carbonate ions in seawater (Tachikawa et al., 1999) observed during equilibrium experiments with synthetic minerals in seawater (Koeppenkastrop and Eric, 1992). The net effect of REE release from particles with a relatively flat shale-normalized REE pattern (with a slight mid-rare earth element (MREE) enrichment) combined with preferential scavenging of LREE results in a shale-normalized REE pattern with a weaker depletion of LREEs and a flat pattern from MREEs to HREEs (Fig. S2).

The scavenged fraction of both Th and LREEs was higher at FAST than at ION. At all stations, scavenged fractions were similar in the D and G treatments. Considering that 3.6 g of dust was introduced in 300 L of seawater, with 17 % to 51 % loss through sedimentation to the bottom trap (Bressac et al., 2011), the average dust concentration remaining in suspension in the tank ranged from 5900 to $9960\,\mu g\,L^{-1}$. This is several orders of magnitude higher than typical particulate matter concentrations in seawater ($1–100\,\mu g\,L^{-1}$; Lal, 1977) not impacted by recent dust deposition events. At these high particulate matter concentrations, it is likely that scavenging of insoluble elements by the remaining suspended dust occurred. Adsorption experiments of a radioactive Ce tracer on deep-sea clays showed a decrease of 30 % in dissolved Ce over a few days (Li et al., 1984), comparable in magnitude to the results presented here. The experiments with deep-sea clays were carried out in abiotic conditions, raising the possibility that adsorption observed during our tank experiments was, at least in part, due to adsorption on the suspended dust. However, since the same dust was used during ION and FAST, it is likely that the higher scavenging rate at FAST compared to ION was due to the higher biological activity at FAST (Gazeau et al., 2020). Th has a high affinity for TEPs (Santschi et al., 2006). However, there was not a marked difference in TEP content at ION compared to FAST (Gazeau et al., 2021). The very high adsorption rates occurred possibly because all the dust was deposited instantaneously at the beginning of the experiment. Deposition of the same amount of dust over longer periods (weeks, months) as in less dusty periods and environments would certainly result in less re-adsorption (but likely similar dissolution).

4.3 Thorium isotopes

The $^{230}Th/^{232}Th$ ratio of surface Mediterranean seawater ($^{230}Th/^{232}Th \approx 15 \times 10^{-6}$; Gdaniec et al., 2018) is higher than the $^{230}Th/^{232}Th$ ratio in the dust ($^{230}Th/^{232}Th \approx 3–6 \times 10^{-6}$; Pham et al., 2005; Roy-Barman et al., 2009). Hence, dust Th release in the tanks leads to a decrease in the $^{230}Th/^{232}Th$ ratio of seawater. Conversely, scavenging of dissolved Th does not lead to changes in the $^{230}Th/^{232}Th$ ratios since both isotopes behave similarly. Hence the $^{230}Th/^{232}Th$ ratios of the seawater allow an esti-

mation of the Th released from dust even when re-adsorption occurs. Further, since the Th content in the dust greatly exceeds the content in seawater, the $^{230}Th/^{232}Th$ ratio in dust remains virtually constant even if seawater-derived Th adsorbs on the particles.

On a diagram of the $^{230}Th/^{232}Th$ ratio as a function of $1/^{232}Th$ (Fig. 6), the theoretical evolution of the filtered seawater samples with time should be as follows: (1) for simple dissolution, filtered seawater samples lie on a straight line between 6×10^{-6} (ratio measured in dust) and 15×10^{-6} (ratio in seawater); (2) if re-adsorption occurs, the filtered seawater samples will be shifted horizontally toward the right (Arraes-Mescoff et al., 2001). For the ION experiments, all C samples (controls with no dust addition) and D and G samples at $t = 1$ h (just after dust addition) plot on an oblique line, suggesting that the initial increase in seawater Th concentration results from the simple dissolution of marine particles. On this diagram, the intercept at $1/^{232}Th = 0$ represents the $^{230}Th/^{232}Th$ of the dissolving particles. This ratio of about $(8.5\pm0.8)\times10^{-6}$ mol mol^{-1} is significantly higher than the ratio measured on the particles ($(6.0\pm0.15)\times10^{-6}$) collected in the traps or in the Saharan dust (Pham et al., 2005; Roy-Barman et al., 2009). It indicates a preferential release of ^{230}Th due to the combined effect of the recoil of two alpha decays from ^{238}U to ^{230}Th and the variable U/Th ratio observed among the phases carrying U and Th in the dust (Bourne et al., 2012; Bosia et al., 2018; Marchandise et al., 2014). Travertine and pedogenic carbonates from the Western Sahara ranges have ^{232}Th concentrations ranging from 0.5 to 12 ppm (Szabo et al., 1995; Candy et al., 2004; Weisrock et al., 2008). Assuming 2 ppm for ^{232}Th in carbonates and considering that carbonate dissolution represents 6.4 % of the dust mass (see Sect. 3.6), an increase of 6.6 pM (1986 pmol in the 300 L tanks) can be estimated, in gross agreement with observations (Fig. 3). While pedogenic calcretes contain sufficient amounts of ^{232}Th and REEs to account for the changes in Th and REE concentrations observed during the PEACETIME experiments (Prudencio et al., 2011), the $^{230}Th/^{232}Th$ ratio of these carbonates is generally low ($^{230}Th/^{232}Th = 2\text{–}5\times10^{-6}$; Candy et al., 2004) so that it cannot account for the higher $^{230}Th/^{232}Th$ ratio ($(8.5\pm0.8)\times10^{-6}$ mol mol^{-1}) found in these experiments (Fig. 6).

Samples from the D and G treatments ($t = 1$ to 72 h) plot on a horizontal line (with little change in the $^{230}Th/^{232}Th$ ratio), confirming that simple reabsorption occurs after the initial dissolution (with little or no release of particulate Th after the initial dissolution observed at $t = 1$ h).

A simple mass balance gives the fraction of dissolved ^{232}Th in seawater from the dissolution of particulate Th (Roy-Barman et al., 2002):

$$f_{\text{litho}} = \frac{\left(\frac{^{230}\text{Th}}{^{232}\text{Th}}\right)_{\text{D or G tank}} - \left(\frac{^{230}\text{Th}}{^{232}\text{Th}}\right)_{\text{C tank}}}{\left(\frac{^{230}\text{Th}}{^{232}\text{Th}}\right)_{\text{dust}} - \left(\frac{^{230}\text{Th}}{^{232}\text{Th}}\right)_{\text{C tank}}}. \quad (3)$$

Knowing f_{litho}, we can determine $f_{\text{dissol\_isot}}$, the dissolution fraction based on the isotopic data:

$$f_{\text{diss\_isot}} = \frac{\text{CONC}_{\text{init}}\left(\frac{f_{\text{litho}}}{1-f_{\text{litho}}}\right)}{\text{CONC}_{\text{dust}} m/V}, \quad (4)$$

where $\text{CONC}_{\text{init}}$ is the ^{232}Th concentration in seawater before dust addition; $f_{\text{dissol\_isot}}$ is independent of concentrations that may be biased by re-adsorption. We evaluate $f_{\text{dissol\_isot}}$ based on average ratios for original seawater (control tanks) and the average ratio of the last samples of the D and G treatments, respectively, to estimate dissolution over the course of the whole experiment (Table S3 in the Supplement). For the particulate ratio, we tentatively used a ratio of 8.5×10^{-6} mol mol^{-1} (value best defined by the y-axis value for $1/^{232}Th = 0$ of the dissolution and scavenging trends at ION; Fig. 5).

The resulting average $f_{\text{dissol\_isot}}$ is below 3 % for FAST and ION treatments D and G, confirming the low solubility of Th (Table 1). While we recognize that for FAST, the large data scatter results in large uncertainties in the interpretation of the results, all the results obtained during PEACETIME indicate a low Th solubility.

4.4 Implication for dust deposition estimation

The $^{230}Th/^{232}Th$ ratio in the surface ocean has been proposed as a tracer to for dust inputs and the release of trace metals at the ocean surface (Hsieh et al., 2011). Neglecting lateral transport, ^{232}Th is delivered by dust dissolution, whereas ^{230}Th derives mostly from the in situ decay of ^{234}U and can be further used to track ^{232}Th dissolution. Knowing the solubility of ^{232}Th would allow the estimation of the dust flux required to account for the $^{230}Th/^{232}Th$ ratio in surface waters. Until now, ^{232}Th solubility from dust was poorly constrained. Using dust fluxes from a global dust deposition model and adjusting the fraction of lithogenic ^{232}Th dissolution to match the $^{230}Th/^{232}Th$ ratio in the surface water of the Atlantic Ocean, Hsieh et al. (2011) estimated that the fraction of lithogenic ^{232}Th dissolution ranges between 1 % and 5 % in high-dust-flux areas such as the eastern equatorial Atlantic and up to 10 %–16 % in areas of low dust deposition such as the South Atlantic (Hsieh et al., 2011). Estimates of the soluble fraction of ^{232}Th at the Bermuda Atlantic Time-series Study (BATS) ranged from 14 % to 28 % and increased with the depth range (Hayes et al., 2017). The solubility of ^{232}Th in atmospheric dust from particle leaching experiments in deionized water or dilute acetic acid provided a wide range of values (Anderson et al., 2016).

The present work indicates a low ^{232}Th fractional solubility (around 1 %) for the dusts used in the tank experiments. It is low but qualitatively consistent with the low solubility (3 %–5 %) of lithogenic Th derived from a budget of Th isotopes in the western Mediterranean Sea, where Th inputs are dominated by ocean margins (Roy-Barman et al., 2002). Our

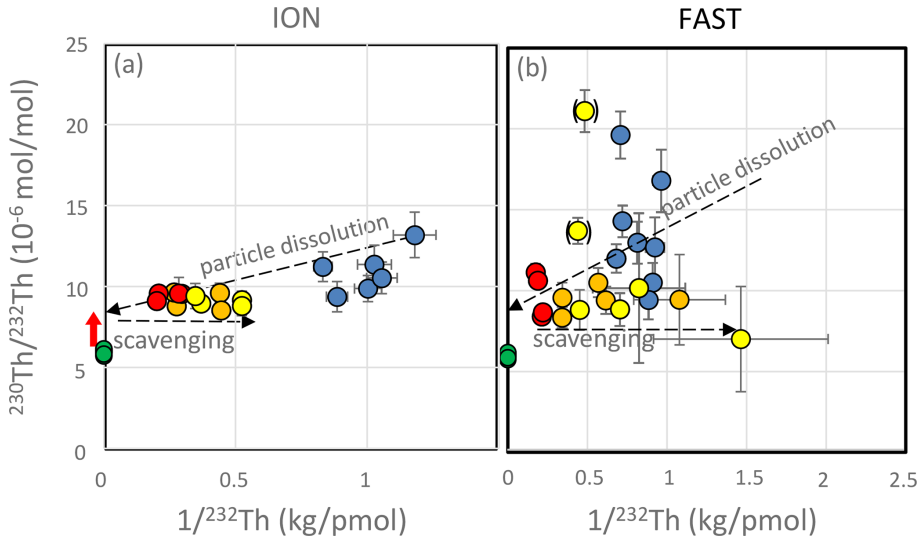

Figure 6. Mixing diagram of $^{230}Th/^{232}Th$ versus $1/^{232}Th$ for the ION **(a)** and FAST **(b)** experiments. Blue dots: $t = 0$ h (no dust addition yet); red dots: $t = 1$–6 h; orange dots: $t = 24$–48 h; yellow dots: $t = 72$–96 h. Yellow dots between brackets fall above the scavenging line for unknown reasons. Green dots: particles in the sediment traps. Red arrow: preferential release of ^{230}Th.

results are also in qualitative accordance with low overall fractional solubility of Th (from 4 % to 8 %) from Saharan aerosols leached with an ammonium acetate solution at pH 4.7 (Baker et al., 2020). Keeping in mind the limitation of our study (limited time duration, very high particle concentration promoting re-adsorption), these results suggest that the high Th solubility derived by balancing dust inputs with the scavenging on settling particles could be biased by advective inputs at large spatial and temporal scales (Hayes et al., 2017). Hence, estimating dust inputs from the $^{230}Th/^{232}Th$ ratio of surface waters (Hsieh et al., 2011) requires the consideration of areas where the water residence time exceeds the Th residence time relative to scavenging. This is the case of part of the South Pacific gyre, where the horizontal dissolved-^{232}Th gradient tends to vanish (Pavia et al., 2020).

One aim of providing ^{230}Th–^{232}Th-based estimates of the dust deposition is to determine Fe fluxes at the ocean surface. To circumvent the difficulty in determining the trace metal solubility from dusts, the relative fractional solubility ratio of Fe to Th (Fe percent dissolution to Th percent dissolution from the dust) is used as a more robust parameter. It is often assumed that Fe and Th are released congruently from dust, yielding an Fe/Th ratio on the order of 20 000 mol mol^{-1} (Hayes et al., 2017, Pavia et al., 2020). Aerosol leaching experiments suggest a preferential release of Th compared to Fe, with an Fe/Th ratio around 10 000 mol mol^{-1} (Baker et al., 2020). Keeping in mind potential bias due to the significantly different dissolution kinetics, a salient result of the PEACETIME tank experiments is the much lower dissolution extent of Fe relative to Th, yielding an upper limit of 200–1500 mol mol^{-1} (Table S5).

5 Conclusions

The PEACETIME tank experiments quantified the particulate-dissolved exchanges of Al, Fe, REEs, Pa and Th following Saharan dust addition to surface seawater from three basins of the Mediterranean Sea under present and future climate conditions. We highlight differences in the amount and kinetics of dissolution as well as scavenging among the different lithogenic tracers and report first estimates for ^{232}Th and ^{231}Pa. Under the experimental conditions, Fe dissolution was much lower than the dissolution of Th, REEs or Al. As a consequence, assuming similar soluble fractions for lithogenic tracers to evaluate Fe fluxes is probably generally not appropriate. Using relative solubility might be also biased by the different dissolution and scavenging kinetics characterizing each tracer. Quite unexpectedly, comparison of present and future conditions indicates that changes in temperature (+3 °C) and/or pH (−0.3 pH) influence the release of ^{232}Th and REEs in seawater, leading to a lower Th release and a higher light REE release under increased greenhouse conditions. Using Th isotopes, we show that Th was released within the first hour of the experiment and that no subsequent Th release occurs during the following days. This observation, associated with the low Th soluble fraction (1 %) from dust, puts constraints on the use of Th isotopes as a tracer of dust inputs in surface waters and highlights the importance of advection as a source of ^{232}Th in the open ocean.

The implications of these experiments are not limited to constraining eolian inputs to the surface ocean. They also contribute to a better understanding of the strong contrast in vertical profiles and zonal distribution of insoluble ele-

ments in the Mediterranean Sea. In this region, dissolved Al increases from the surface to deep waters and also laterally at depth from the western basin to the eastern basin (Rolison et al., 2015). Dissolved Fe and ^{232}Th profiles often present surface concentration maxima but no systematic concentration gradient between the deep western and eastern basins (Gerringa et al., 2017; Gdaniec et al., 2018). While the fractions of Al and Th dissolved from dust during the tank experiments were comparable, dissolution kinetics were different: ^{232}Th was largely removed through scavenging after the initial release, whereas Al increased continuously in the tanks. This highlights the highly particle-reactive character of ^{232}Th as compared to Al. Hence ^{232}Th cannot accumulate along the Mediterranean deep circulation and does not exhibit a zonal gradient as Al.

Data availability. Underlying research data are being used by researcher participants of the "Peacetime" campaign to prepare other manuscripts, and therefore data are not publicly accessible at the time of publication. Data will be accessible (http://www.obs-vlfr.fr/proof/php/PEACETIME/peacetime.php, Guieu et al., 2020b) once the special issue is completed (all papers should be published by fall 2020).

Supplement. The supplement related to this article is available online at: https://doi.org/10.5194/bg-18-2663-2021-supplement.

Author contributions. CG and KD conceived the PEACETIME program. CG and FG conceived and led the tank experiments on board. MB analyzed dissolved Fe. TW analyzed dissolved Al. NL analyzed trapped material. MRB, LF and ED analyzed Th, Pa and REEs. MRB prepared the manuscript with contributions from all co-authors.

Competing interests. The authors declare that they have no conflict of interest.

Special issue statement. This article is part of the special issue "Atmospheric deposition in the low-nutrient–low-chlorophyll (LNLC) ocean: effects on marine life today and in the future (ACP/BG interjournal SI)". It is not associated with a conference.

Acknowledgements. This study is a contribution to the PEACETIME project (http://peacetime-project.org, last access: 9 April 2021), a joint initiative of the MERMEX and ChArMEx components supported by the CNRS-INSU, IFREMER, CEA and Météo-France as part of the MISTRALS program coordinated by CNRS-INSU (PEACETIME cruise; https://doi.org/10.17600/17000300). All data have been acquired during the PEACETIME oceanographic expedition on board R/V *Pourquoi Pas?* in May–June 2017. PEACETIME was endorsed as a process study by GEOTRACES. PEACETIME is also a contribution to the SOLAS and IMBER programs. We thank the captain and the crew of the RV *Pourquoi Pas?* for their professionalism and their work at sea. Frank Pavia, an anonymous reviewer and co-editor-in-chief Christine Klaas greatly improved this paper with their constructive comments.

Financial support. Matthieu Bressac received a grant from the European Union Seventh Framework Program (grant no. PIOF-GA-2012-626734). The publication of this article was financed by the CNRS-INSU.

Review statement. This paper was edited by Christine Klaas and reviewed by Frank Pavia and one anonymous referee.

References

Anderson, R. F., Fleisher, M. Q., Robinson, L., Edwards, R. L., Hoff, J. A., Moran, S. B., Rutgers van der Loeff, M. M., Thomas, A. L., Roy-Barman, M., and Francois, R.: GEOTRACES intercalibration of ^{230}Th, ^{232}Th, ^{231}Pa, and prospects for ^{10}Be, Limnol. Oceanogr.-Meth., 10, 179–213, 2012.

Anderson, R. F., Cheng, H., Edwards, R. L., Fleisher, M. Q., Hayes, C. T., Huang, K. F., Kadko, D., Lam, P. J., Landing, W. M., Lao, Y., Lu, Y., Measures, C. I., Morton, P. L., Moran, S. B., Robinson, L. F., and Shelley, R. U.: How well can we quantify dust deposition to the ocean?, Philos. T. R. Soc. A, 374, 2015028520150285, https://doi.org/10.1098/rsta.2015.0285, 2016.

Aghnatios, C., Losno, R., and Dulac, F.: A fine fraction of soil used as an aerosol analogue during the DUNE experiment: sequential solubility in water, decreasing pH step-by-step, Biogeosciences, 11, 4627–4633, https://doi.org/10.5194/bg-11-4627-2014, 2014.

Arraes-Mescoff, R., Roy-Barman, M., Coppola, L., Souhaut, M., Tachikawa, K., Jeandel, C., Sempéré, R., and Yoro, C.: The behavior of Al, Mn, Ba, Sr, REE and Th isotopes during in vitro degradation of large marine particles, Mar. Chem., 73, 1–19, 2001.

Azetsu-Scott, K. and Niven, S. E.: The role of transparent exopolymer particles (TEP) in the transport of ^{234}Th in coastal water during a spring bloom, Cont. Shelf Res., 25, 1133–1141, 2005.

Baker, A. R. and Croot, P. L.: Atmospheric and marine controls on aerosol iron solubility in seawater, Mar. Chem., 120, 4–13, 2010.

Baker, A. R., Li, M., and Chance, R.: Trace metal fractional solubility in size-segregated aerosols from the tropical eastern Atlantic Ocean, Global Biogeochem. Cy., 34, e2019GB006510, https://doi.org/10.1029/2019GB006510, 2020.

Bosia, C., Chabaux, F., Pelt, E., Cogez, A., Stille, P., Deloule, E., and France-Lanord, C.: U-series disequilibria in minerals from Gandak River sediments (Himalaya), Chem. Geol., 477, 22–34, 2018.

Bonnet, S. and Guieu, C.: Atmospheric forcing on the annual iron cycle in the western Mediterranean Sea: A 1 year survey, J. Geophys. Res.-Oceans, 111, C09010, https://doi.org/10.1029/2005JC003213, 2006.

Bourne, M. D., Thomas, A. L., Mac Niocaill, C., and Henderson, G. M.: Improved determination of marine sedimentation

rates using ^{230}Thxs, Geochem. Geophy. Geosy., 13, Q09017, https://doi.org/10.1029/2012GC004295, 2012.

Bressac, M. and C. Guieu: Post-depositional processes: What really happens to new atmospheric iron in the ocean's surface?, Global Biogeochem. Cy., 27, 859–870, 2013.

Bressac, M., Guieu, C., Doxaran, D., Bourrin, F., Obolensky, G., and Grisoni, J. M.: A mesocosm experiment coupled with optical measurements to assess the fate and sinking of atmospheric particles in clear oligotrophic waters, Geo-Mar. Lett., 32, 153–164, 2012.

Bressac, M., Wagener, T., Leblond, N., Tovar-Sánchez, A., Ridame, C., Albani, S., Guasco, S., Dufour, A., Jacquet, S., Dulac, F., Desboeufs, K., and Guieu, C.: Subsurface iron accumulation and rapid aluminium removal in the Mediterranean following African dust deposition, Biogeosciences Discuss., https://doi.org/10.5194/bg-2021-87, in review, 2021.

Candy, I., Black, S., and Sellwood, B. W.: Quantifying time scales of pedogenic calcrete formation using U-series disequilibria, Sediment. Geol., 170, 177–187, 2004.

Censi, P., Mazzola, S., Sprovieri, M., Bonanno, A., Patti, B., Punturo, R., Spoto, S. E., Saiano, F., and Alonzo, G.: Rare earth elements distribution in seawater and suspended particulate of the Central Mediterranean Sea, Chem. Ecol., 20, 323–343, 2004.

Desboeufs, K. V., Losno, R., and Colin, J. L.: Factors influencing aerosol solubility during cloud process, Atmos. Environ., 35, 3529–3537, 2001.

Desboeufs, K., Sofikitis, A., Losno, R., Colin, J. L., and Ausset, P.: Trace metals dissolution and solubility from mineral particles, Chemosphere, 58, 195–203, 2005.

Desboeufs, K., Leblond, N., Wagener, T., Bon Nguyen, E., and Guieu, C.: Chemical fate and settling of mineral dust in surface seawater after atmospheric deposition observed from dust seeding experiments in large mesocosms, Biogeosciences, 11, 5581–5594, https://doi.org/10.5194/bg-11-5581-2014, 2014.

Duce, R. A. and Tindale, N. W.: Atmospheric transport of iron and its deposition in the ocean, Limnol. Oceanogr., 36, 1715–1726, 1991.

Fu, F., Desboeufs, K., Triquet, S., Doussin, J.-F., Giorio, C., Formenti, P., Feron, A., Maisonneuve, F., and Dulac, F.: Aerosol characterisation and quantification of trace element atmospheric dry deposition fluxes in remote Mediterranean Sea during PEACETIME cruise, Atmosph. Chem. Phys., this special Issue, in preparation, 2021.

Gazeau, F., Ridame, C., Van Wambeke, F., Alliouane, S., Stolpe, C., Irisson, J.-O., Marro, S., Grisoni, J.-M., De Liège, G., Nunige, S., Djaoudi, K., Pulido-Villena, E., Dinasquet, J., Obernosterer, I., Catala, P., and Guieu, C.: Impact of dust enrichment on Mediterranean plankton communities under present and future conditions of pH and temperature: an experimental overview, Biogeosciences Discuss., https://doi.org/10.5194/bg-2020-202, in review, 2020.

Gazeau, F., Van Wambeke, F., Marañón, E., Pérez-Lorenzo, M., Alliouane, S., Stolpe, C., Blasco, T., Leblond, N., Zäncker, B., Engel, A., Marie, B., Dinasquet, J., and Guieu, C.: Impact of dust addition on the metabolism of Mediterranean plankton communities and carbon export under present and future conditions of pH and temperature, Biogeosciences Discuss., https://doi.org/10.5194/bg-2021-20, in review, 2021.

Gehlen, M., Beck, L., Calas, G., Flank, A. M., Van Bennekom, A. J., and Van Beusekom, J. E. E.: Unraveling the atomic structure of biogenic silica: evidence of the structural association of Al and Si in diatom frustules, Geochim. Cosmochim. Ac., 66, 1601–1609, 2002.

Gerringa, L. J. A., Slagter, H. A., Bown, J., van Haren, H., Laan, P., De Baar, H. J. W., and Rijkenberg, M. J. A.: Dissolved Fe and Fe-binding organic ligands in the Mediterranean Sea–GEOTRACES G04, Mar. Chem., 194, 100–113, 2017.

Gdaniec, S., Roy-Barman, M., Foliot, L., Thil, F., Dapoigny, A., Burckel, P. A., Masque, P., Garcia-Orellana, J., Morth, M., and Andersson, P. S.: Thorium and protactinium isotopes as tracers of marine particle fluxes and deep water circulation in the Mediterranean Sea, Mar. Chem., 199, 12–23, 2018.

Greaves, M. J., Statham, P. J., and Elderfield, H.: Rare earth element mobilization from marine atmospheric dust into seawater, Mar. Chem., 46, 255–260, 1994.

Greaves, M. J., Elderfield, H., and Sholkovitz, E. R.: Aeolian sources of rare earth elements to the Western Pacific Ocean, Mar. Chem., 68, 31–38, 1999.

Guieu, C.: Iron from a submarine source impacts the productive layer of the Western Tropical South Pacific (WTSP), Sci. Rep., 8, 9075, https://doi.org/10.1038/s41598-018-27407-z, 2018.

Guieu, C., Roy-Barman, M., Leblond, N., Jeandel, C., Souhaut, M., Le Cann, B., Dufour, A., and Bournot, C.: Vertical particle flux in the northeast Atlantic Ocean (POMME experiment), J. Geophys. Res.-Oceans, 110, 1–21, https://doi.org/10.1029/2004JC002672, 2005.

Guieu, C., Dulac, F., Desboeufs, K., Wagener, T., Pulido-Villena, E., Grisoni, J.-M., Louis, F., Ridame, C., Blain, S., Brunet, C., Bon Nguyen, E., Tran, S., Labiadh, M., and Dominici, J.-M.: Large clean mesocosms and simulated dust deposition: a new methodology to investigate responses of marine oligotrophic ecosystems to atmospheric inputs, Biogeosciences, 7, 2765–2784, https://doi.org/10.5194/bg-7-2765-2010, 2010a.

Guieu, C., Loÿe-Pilot, M. D., Benyahya, L., and Dufour, A.: Spatial variability of atmospheric fluxes of metals (Al, Fe, Cd, Zn and Pb) and phosphorus over the whole Mediterranean from a one-year monitoring experiment: Biogeochemical implications, Mar. Chem., 120, 164–178, https://doi.org/10.1016/j.marchem.2009.02.004, 2010b.

Guieu, C., D'Ortenzio, F., Dulac, F., Taillandier, V., Doglioli, A., Petrenko, A., Barrillon, S., Mallet, M., Nabat, P., and Desboeufs, K.: Introduction: Process studies at the air–sea interface after atmospheric deposition in the Mediterranean Sea – objectives and strategy of the PEACETIME oceanographic campaign (May–June 2017), Biogeosciences, 17, 5563–5585, https://doi.org/10.5194/bg-17-5563-2020, 2020a.

Guieu, C., Desboeufs, K., Albani, S., Alliouane, S., Aumont, O., Barbieux, M., Barrillon, S., Baudoux, A.-C., Berline, L., Bhairy, N., Bigeard. E., Bloss, M., Bressac, M., Brito, J., Carlotti, F., de Liege, G., Dinasquet, J., Djaoudi, K., Doglioli, A., D'Ortenzio, F., Doussin, J.-F., Duforet, L., Dulac, F., Dutay, J.-C., Engel, A., Feliu-Brito, G., Ferre, H., Formenti, P., Fu, F., Garcia, D., Garel, D., Gazeau, F., Giorio, C., Gregori, G., Grisoni, J.-M., Guasco, S., Guittonneau, J., Haëntjens, N., Heimburger, L.-E., Helias, S., Jacquet, S., Laurent, B., Leblond, N., Lefevre, D., Mallet , M., Marañón, E., Nabat, P., Nicosia, A., Obernosterer, I., Perez, L., M., Petrenko, A., Pulido-Villena, E., Raimbault, P., Ridame, C.,

Riffault, V., Rougier, G., Rousselet, L., Roy-Barman, M., Saiz-Lopez, A., Schmechtig, C., Sellegri, K., Siour, G., Taillandier, V., Tamburini , C., Thyssen, M., Tovar-Sanchez, A., Triquet, S., Uitz, J., Van Wambeke, F., Wagener, T., and Zaencker, B.: Biogeochemical dataset collected during the PEACETIME cruise, SEANOE [Dataset], https://doi.org/10.17882/75747 (last access: 16 April 16 2021), 2020b.

Haley, B. A., Klinkhammer, G. P., and McManus, J.: Rare earth elements in pore waters of marine sediments, Geochim. Cosmochim. Ac., 68, 1265–1279, 2004.

Hayes, C. T., Rosen, J., McGee, D., and Boyle, E. A.: Thorium distributions in high-and low-dust regions and the significance for iron supply, Global Biogeochem. Cy., 31, 328–347, 2017.

Hsieh, Y. T., Henderson, G. M., and Thomas, A. L.: Combining seawater ^{232}Th and ^{230}Th concentrations to determine dust fluxes to the surface ocean, Earth Planet. Sci. Lett., 312, 280–290, 2011.

Hydes, D. J. and Liss, P. S.: Fluorimetric method for the determination of low concentrations of dissolved aluminium in natural waters, Analyst, 101, 922–931, 1976.

Jickells, T. D., An, Z. S., Andersen, K. K., Baker, A. R., Bergametti, G., Brooks, N., Cao, J. J., Boyd, P. W., Duce, R. A., Hunter, K. A.,Kawahata, H., Kubilay, N., laRoche, J., Liss, P. S., Mahowald, N., Prospero, J. M., Ridgwell, A. J., Tegen, I., and Torres, R.: Global iron connections between desert dust, ocean biogeochemistry, and climate, Science 308, 67–71, 2005.

Koeppenkastrop, D. and Eric, H.: Sorption of rare-earth elements from seawater onto synthetic mineral particles: An experimental approach, Chem. Geol., 95, 251–263, 1992.

Lal, D.: The oceanic microcosm of particles, Science, 198, 997–1009, 1977.

Li, Y. H., Burkhardt, L., Buchholtz, M., O'Hara, P., and Santschi, P. H: Partition of radiotracers between suspended particles and seawater, Geochim. Cosmochim. Ac., 48, 2011–2019, 1984.

Louis, J., Gazeau, F., and Guieu, C.: Atmospheric nutrients in seawater under current and high pCO_2 conditions after Saharan dust deposition: Results from three tank experiments, Prog. Oceanogr., 163, 40–49, 2018.

Loÿe-Pilot, M. D. and Martin, J. M.: Saharan dust input to the western Mediterranean: an eleven years record in Corsica, in: The impact of desert dust across the Mediterranean, Springer, Dordrecht, 191–199, 1996.

Marchandise, S., Robin, E., Ayrault, S., and Roy-Barman, M.: U−Th−REE−Hf bearing phases in Mediterranean Sea sediments: Implications for isotope systematics in the ocean, Geochim. Cosmochim. Ac., 131, 47–61, 2014.

Measures, C. I. and Vink, S.: On the use of dissolved aluminum in surface waters to estimate dust deposition to the ocean, Global Biogeochem. Cy., 14, 317–327, 2000.

Millero, F. J.: Solubility of Fe(III) in seawater, Earth Planet. Sci. Lett., 154, 323–329, 1998.

Paris, R., Desboeufs, K. V., Formenti, P., Nava, S., and Chou, C.: Chemical characterisation of iron in dust and biomass burning aerosols during AMMA-SOP0/DABEX: implication for iron solubility, Atmos. Chem. Phys., 10, 4273–4282, https://doi.org/10.5194/acp-10-4273-2010, 2010.

Paris, R., Desboeufs, K., and Journet, E.: Variability of dust iron solubility in atmospheric waters: Investigation of the role of oxalate organic complexation, Atmos. Environ., 45, 6510–6517, 2011.

Pavia, F. J., Anderson, R. F., Winckler, G. and Fleisher, M. Q.: Atmospheric Dust Inputs, Iron Cycling, and Biogeochemical Connections in the South Pacific Ocean from Thorium Isotopes, Global Biogeochem. Cy., 34, e2020GB006562, https://doi.org/10.1029/2020GB006562, 2020.

Pham, M. K., La Rosa, J. J., Lee, S. H., Oregioni, B., and Povinec, P. P.: Deposition of Saharan dust in Monaco rain 2001–2002: radionuclides and elemental composition, Phys. Scripta, 2005(T118), 14, 2005.

Prudêncio, M. I., Dias, M. I., Waerenborgh, J. C., Ruiz, F., Trindade, M. J., Abad, M., Marques, R., and Gouveia, M. A.: Rare earth and other trace and major elemental distribution in a pedogenic calcrete profile (Slimene, NE Tunisia), Catena, 87, 147–156, 2011.

Rolison, J. M., Middag, R., Stirling, C. H., Rijkenberg, M. J. A., and De Baar, H. J. W.: Zonal distribution of dissolved aluminium in the Mediterranean Sea, Mar. Chem. 177, 87–100, 2015.

Roy-Barman, M., Coppola, L., and Souhaut, M.: Thorium isotopes in the western Mediterranean Sea: An insight into the marine particle dynamics, Earth Planet. Sci. Lett. 196, 161–174, https://doi.org/10.1016/S0012-821X(01)00606-9, 2002.

Roy-Barman, M., Lemaître, C., Ayrault, S., Jeandel, C., Souhaut, M., and Miquel, J. C.: The influence of particle composition on Thorium scavenging in the Mediterranean Sea, Earth Planet. Sci. Lett., 286, 526–534, https://doi.org/10.1016/j.epsl.2009.07.018, 2009.

Santschi, P. H., Murray, J. W., Baskaran, M., Benitez-Nelson, C. R., Guo, L. D., Hung, C. C., Lamborg, C., Moran, S. B., Passow, U., and Roy-Barman, M.: Thorium speciation in seawater, Mar. Chem., 100, 250–268, 2006.

Savenko, A. V. and Savenko, V. S.: Aluminum hydroxide's solubility and the forms of dissolved aluminum's occurrence in seawater, Oceanology, 51, 231–234, 2011.

Szabo, B. J., Haynes Jr, C. V., and Maxwell, T. A.: Ages of Quaternary pluvial episodes determined by uranium-series and radiocarbon dating of lacustrine deposits of Eastern Sahara, Palaeogeogr. Palaeocl., 113, 227–242, 1995.

Tachikawa, K., Jeandel, C., and Roy-Barman, M.: A new approach to the Nd residence time in the ocean: the role of atmospheric inputs, Earth Planet. Sci. Lett., 170, 433–446, 1999.

Tachikawa, K., Roy-Barman, M., Michard, A., Thouron, D., Yeghicheyan, D., and Jeandel, C.: Neodymium isotopes in the Mediterranean Sea: comparison between seawater and sediment signals, Geochim. Cosmochim. Ac., 68, 3095–3106, 2004.

Taylor, S. R. and McLennan, S. M.: The geochemical evolution of the continental crust, Rev. Geophys. 33, 241–265, 1995.

Ternon, E., Guieu, C., Loÿe-Pilot, M.-D., Leblond, N., Bosc, E., Gasser, B., Miquel, J.-C., and Martín, J.: The impact of Saharan dust on the particulate export in the water column of the North Western Mediterranean Sea, Biogeosciences, 7, 809–826, https://doi.org/10.5194/bg-7-809-2010, 2010.

Twining, B. S., Rauschenberg, S., Morton, P. L., and Vogt, S.: Metal contents of phytoplankton and labile particulate material in the North Atlantic Ocean, Progr. Oceanogr., 137, 261–283, 2015.

van de Flierdt, T., Pahnke, K., Amakawa, H., Andersson, P., Basak, C., Coles, B., Colin, C.,Crocket, K., Frank, M., Frank, N., Goldstein, S. L., Goswami, V., Haley, B. A., Hathorne, E. C., Hemming, S. R., Henderson, G. M., Jeandel, C., Jones, K., Kreissig, K., Lacan, F., Lambelet, M., Martin, E. E., Newkirk, D. R.,

Obata, H., Pena, L., Piotrowski, A. M.,Pradoux, C., Scher, H. D., Schöbert, H., Singh, S. K., Stichel, T., Tazoe, H., Vance, D., and Yang, J.: GEOTRACES intercalibration of neodymium isotopes and rare earth element concentrations in seawater and suspended particles, Part 1: reproducibility of results for the international intercomparison, Limnol. Oceanogr.-Meth., 10, 234–251, 2012.

Van Wambeke, F., Taillandier, V., Deboeufs, K., Pulido-Villena, E., Dinasquet, J., Engel, A., Marañón, E., Ridame, C., and Guieu, C.: Influence of atmospheric deposition on biogeochemical cycles in an oligotrophic ocean system, Biogeosciences Discuss. [preprint], https://doi.org/10.5194/bg-2020-411, in review, 2020.

Wagener, T., Pulido-Villena, E., and Guieu, C.: Dust iron dissolution in seawater: Results from a one-year time-series in the Mediterranean Sea, Geophys. Res. Lett., 35, https://doi.org/10.1029/2008GL034581, 2008.

Wagener, T., Guieu, C., and Leblond, N.: Effects of dust deposition on iron cycle in the surface Mediterranean Sea: results from a mesocosm seeding experiment, Biogeosciences, 7, 3769–3781, https://doi.org/10.5194/bg-7-3769-2010, 2010.

Witter, A. E., Hutchins, D. A., Butler, A., and Luther III, G. W.: Determination of conditional stability constants and kinetic constants for strong model Fe-binding ligands in seawater, Mar. Chem., 69, 1–17, 2000.

Weisrock, A., Rousseau, L., Reyss, J. L., Falguères, C., Ghaleb, B., Bahain, J. J., Beauchamp, J., Boudad, L., Mercier, N., Mahieux, G., Pozzi, J.-P., Janati-Idrissi, N., and Ouammou, A.: Travertines of the Moroccan Sahara northern border: morphological settings, U-series datings and palaeoclimatic indications, Geomorphologie, 4, 153–168, 2008.